


SiRNF8 Delivered by DNA Framework Nucleic Acid Effectively Sensitizes Chemotherapy in Colon Cancer

Zhao Guo^{1,*}, Haoyun Song^{1,*}, Yingxia Tian^{2,*}, Jie Xu³, Guokun Zhang¹, Yanan Guo¹, Rong Shen¹, Degui Wang¹ 

¹Department of Anatomy and Histology, Lanzhou University School of Basic Medical Sciences, Lanzhou, 730000, People's Republic of China;

²Department of Internal Medicine, Gansu Provincial Academic Institute for Medical Research, Lanzhou, 730050, People's Republic of China; ³Cuiying Biomedical Research Center, Lanzhou University Second Hospital, Lanzhou, Gansu, 730030, People's Republic of China

*These authors contributed equally to this work

Correspondence: Degui Wang; Rong Shen, Department of Anatomy and Histology, Lanzhou University School of Basic Medical Sciences, Lanzhou, 730000, People's Republic of China, Tel +86 13893609120; +86 13909483373, Fax +86 931 8915023, Email wangdegui@lzu.edu.cn; shenr@lzu.edu.cn

Background: The evident side effects and decreased drug sensitivity significantly restrict the use of chemotherapy. However, nanoparticles based on biomaterials are anticipated to address this challenge.

Methods: Through bioinformatics analysis and colon cancer samples, we initially investigated the expression level of RNF8 in colon cancer. Next, we constructed nanocarrier for delivering siRNF8 based on DNA tetrahedron (si-Tet), and Doxorubicin (DOX) was further intercalated into the DNA structure (si-DOX-Tet) for combination therapy. Further, the effects and mechanism of RNF8 inhibition on the sensitivity of colon cancer cells to DOX chemotherapy have also been studied.

Results: RNF8 expression was increased in colon cancer. Agarose gel electrophoresis, transmission electron microscopy, and size distribution and potential analysis confirmed the successful preparation of the two nanoparticles, with particle sizes of 10.29 and 37.29 nm, respectively. Fluorescence imaging reveals that the carriers can be internalized into colon cancer cells and escape from lysosomes after 12 hours of treatment, effectively delivering siRNF8 and DOX. Importantly, Western blot analysis verified treatment with 50nM si-Tet silenced RNF8 expression by approximately 50% in colon cancer cells, and combined treatment significantly inhibited cell proliferation. Furthermore, the CCK-8 assay demonstrated that si-Tet treatment enhanced the sensitivity of colon cancer cells to the three chemotherapeutic drugs. Significant more DNA damage was detected after treatment with both si-Tet or si-DOX-Tet. Further flow cytometry analysis revealed that si-DOX-Tet treatment led to significantly more apoptosis, approximately 1.6-fold higher than treatment with DOX alone. Mechanistically, inhibiting RNF8 led to decreased ABCG2 expression and DOX efflux, but increased DNA damage, thereby enhancing the chemotherapeutic effect of DOX.

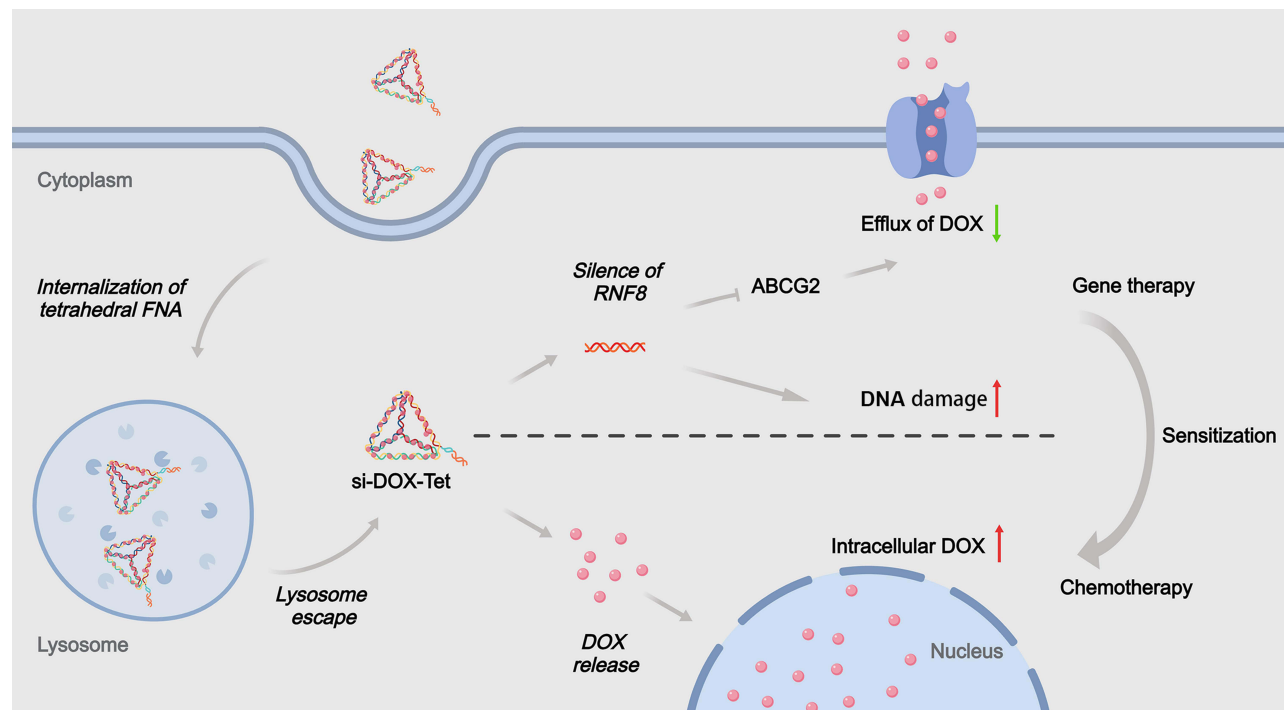
Conclusion: We have successfully constructed si-DOX-Tet. By inhibiting the expression of RNF8, it enhances the chemotherapy sensitivity of DOX. Therefore, this tetrahedral FNA nanocarrier offers a new approach for the combined treatment of colon cancer.

Keywords: DNA framework nucleic acid, RNF8, chemosensitivity, RNAi, colorectal cancer

Introduction

Colorectal cancer (CRC) is now the third most prevalent malignant tumor and the second leading cause of cancer-related mortality among 36 cancer types across 185 countries worldwide, according to the most recent global cancer burden data published by the International Agency for Research on Cancer of the World Health Organization.^{1,2} Adjuvant and neoadjuvant chemotherapy play crucial roles in the treatment of CRC. Recent advancements in chemotherapy have markedly enhanced the short-term outcomes of cancer. Nevertheless, severe side effects and reduced chemosensitivity are the primary causes of treatment failure.³⁻⁵ Doxorubicin (DOX) or Doxil[®] is a potent anthracycline antibiotic extensively researched for its potential in treating various cancers, including CRC, and has shown encouraging anticancer effects.⁶⁻⁸ DOX can intercalate into DNA, thereby inhibiting DNA synthesis,

Graphical Abstract



causing DNA damage, and inducing apoptosis in cancer cells.^{9,10} However, due to its short half-life and poor tissue targeting, high doses of DOX are usually required to effectively kill cancer cells, resulting in cytotoxicity and serious side effects (especially irreversible cardiotoxicity), accompanied by the development of drug resistance, limiting its clinical application.¹¹ Statistically, cardiotoxicity induced by DOX occurs in as many as 25% of patients.¹² Excessive oxidative stress, DNA double-strand breaks (DSBs) resulting from topoisomerase 2 (Top2) poisoning, and mitochondrial damage are the primary contributors of damage to cardiomyocytes, leading to cardiotoxicity through various mechanisms such as autophagy, apoptosis, ferroptosis, and pyroptosis.^{12,13} Damaged myocardium causes progressive decrease of left ventricular ejection fraction, thinning of ventricular walls, arrhythmia, and even heart failure, which ultimately leads to an increased risk of death in cancer patients.^{8,12} Hence, there is a pressing requirement to devise more efficient chemotherapy sensitization strategies to increase the therapeutic effect and improve the prognosis and long-term survival of CRC patients.

Ubiquitination involves the attachment of ubiquitin molecules to substrate proteins through a series of ubiquitinating enzymes, including E1, E2, and E3,¹⁴ thereby regulating protein activity, cellular localization, interaction with other proteins and protein stability.^{15–17} It is extensively involved in a range of human diseases such as neurodegenerative diseases, inflammation, and cancer.^{15–17} The fate of the substrate proteins is determined by the distinct linkage of the mono- and/or polyubiquitin chains. For instance, K48-linked ubiquitination primarily facilitates the proteasomal degradation of substrate proteins, whereas K63-linked ubiquitination has been demonstrated to activate protein functions and engage in signaling pathways.^{18–20} Increased K63-linked ubiquitination has been reported to overactivate oncogenic signaling and promote tumor progression.²¹ RNF8 is classified as a ring finger E3 ligase, and numerous studies have elucidated its specific roles in DNA damage repair, regulation of cell cycle progression, and protection of telomere ends.^{16,17} Clearly, RNF8 deficiency leads to genomic instability and tumorigenesis in mice.^{16,22} However, recent studies have reported that RNF8 promotes cancer progression, including epithelial-mesenchymal transition (EMT), metastasis and chemotherapy resistance.^{23–27} Ren et al reported that RNF8 promoted colon cancer proliferation by binding β -catenin and promoting its nuclear translocation through K63 polyubiquitination, consequently inducing c-Myc expression.²³ Another study revealed that RNF8 is overexpressed in lung cancer, which regulates Akt activation through K63-linked ubiquitination, leading to lung cancer cell proliferation and chemoresistance, and positively correlated with poor survival of

non-small cell lung cancer (NSCLC) patients.²⁷ Similarly, in Lee's study, they reported that RNF8 was upregulated in breast cancer, and RNF8 could directly activate Twist (an important transcription factor in EMT) via K63-linked ubiquitylation, which further causes Twist to localize to the nucleus to play a cancer-promoting role, leading to the development of chemotherapy resistance.²⁸ Therefore, RNF8 may be an effective target for sensitizing chemotherapy, and inhibition of RNF8 may improve the efficacy of chemotherapy in individuals with CRC.

In recent years, numerous studies have highlighted the prospect of nanocarriers in the diagnosis and treatment of CRC, including iron oxide nanocrystals, quantum dots, poly (lactic-co-glycolic acid) NPs, dendrimers, carbon nanotubes, liposomes, silica NPs, gold NPs, DNA nanotechnology, nanoemulsion system, etc.^{11,29–32} Based on the distinct properties of different nanocarriers, generally, inorganic nanoparticles are typically well-suited for cancer imaging owing to their robust stability and minimal biodegradability. Conversely, organic nanoparticles, while less stable, exhibit high biocompatibility and can be utilized for drug delivery following suitable modification.³⁰ Nanoparticles can be designed in diverse sizes and structures to enhance drug solubility and biostability, facilitate drug targeting and controlled release, and ultimately achieve increased tumor accumulation and prolonged blood circulation times.^{33–35} Compared with traditional treatment, it improves the diagnosis and treatment effect and the survival chance of CRC patients.^{29,33} Structural DNA nanotechnology, initially introduced by Ned Seeman, enables DNA to be folded into a wide variety of shapes through pre-design and strict base complementary pairing.^{36–39} Examples include DNA tetrahedron, DNA prism, DNA nanotube and planar DNA origami.^{40,41} DNA nanostructure technology offers several advantages, including pre-designed shape, easy surface modification and high biocompatibility.^{42–44} And with high drug loading capacity, DNA nanostructure is considered as a safe and effective drug delivery system for CRC treatment.^{41,45} For example, Jorge et al fused DNA tetrahedron with 5-fluoro-2'-deoxyuridine oligomers (FdU_n) for the treatment of CRC cells, which notably increased the therapeutic sensitivity of the cells. Compared to conventional 5-FU and FdU, FdU_n modified DNA nanostructures induced a higher rate of CRC cell apoptosis and demonstrated increased cytotoxicity.⁴⁶ Given the pivotal roles of RNF8 in DNA damage repair, apoptosis and chemosensitivity, we aimed to develop new strategies to sensitize DOX chemotherapy and reduce its toxic side effects by inhibiting RNF8 with siRNA using DNA nanostructure as a carrier. In contrast to the electrostatic loading of siRNA on the surface of cationic inorganic nanoparticles, the complementary DNA-DNA binding allows for the easy integration of small RNA fragments into DNA nanostructures without the need for chemical modification. This feature is advantageous in reducing siRNA leakage during transport, making it a promising candidate for siRNA delivery.^{47–50}

In the current study, we aim to utilize DNA tetrahedron (Tet) as the core to design and construct si-Tet and si-DOX-Tet. The former involves linking siRNF8 to the DNA tetrahedral core via a stretch of DNA, while the latter is loaded with DOX on top of this. The nanoparticles were characterized using gel electrophoresis, size distribution and zeta potential analysis, and transmission electron microscopy (TEM). We conducted further analysis of their interactions with cells and confirmed safety and efficacy *in vitro*. RNF8 can be effectively silenced by si-Tet, which increases the chemotherapy sensitivity of DOX in the treatment of colon cancer cells. The combined effect of the two can also more effectively inhibit colon cancer cells. In summary, si-DOX-Tet is an effective platform for tumor treatment as it integrates gene silencing and chemotherapy.

Materials and Methods

Materials and Cell Lines

All DNA and RNA sequences used for the assembly of FNAs were synthesized and purified by Sangon Biotech (Shanghai) Co., Ltd., and dissolved in ultrapure water to 50 μ M and stored at -20°C . Primers were also synthesized by Sangon Biotech (Shanghai) Co., Ltd. RIPA buffer (high), PMSF, SDS-PAGE loading buffer, 30% acrylamide-bisacrylamide, agarose, Tris, EDTA- Na_2 , ECL Western Blotting Substrate, ammonium persulphate, Hoechst 33342 Stain solution, Lyso-Tracker Green, CCK-8 Cell Proliferation and Cytotoxicity Assay Kit, Annexin V PE/7-AAD, Penicillin-Streptomycin Liquid were purchased from Beijing Solarbio Science & Technology Co., Ltd. RPMI 1640, fetal bovine serum, TRIzol RNA Isolation Reagents and PageRuler™ Prestained Protein Ladder were purchased from Thermo Fisher Scientific Inc. DNA Marker I, SuperReal PreMix Plus (SYBR Green), FastKing gDNA Dispelling RT SuperMix were purchased from TIANGEN Biotech(Beijing) Co.,Ltd. All primary and secondary antibodies were purchased from Proteintech Group, Inc. The universal SAP kit (mouse/rabbit universal) was purchased from ZSGB-BIO. Doxorubicin hydrochloride, oxaliplatin, and 5-fluorouracil were purchased from MedChemExpress. Ethanol,

isopropanol, magnesium acetate, glacial acetic acid, and magnesium chloride were purchased from Damao Chemical Reagent Factory. All reagents were analytical reagents. The solvent used in the experiments was ultrapure water.

Human normal colonic epithelial cell FHC as well as four human colon cancer cell lines (HCT116/RKO/SW480/SW620) were obtained from the American Type Culture Collection (ATCC, Rockville, Maryland, USA). All cells were cultured in RPMI 1640 medium containing 10% fetal bovine serum in an incubator with a carbon dioxide concentration of 5% and a constant temperature of 37°C. Short tandem repeat signatures were identified for each cell line.

The tissue microarray, containing 96 samples from 48 cases, was purchased from Shanghai Wellbio Company for immunohistochemical staining. In addition, 20 samples were collected from 10 cases of colon cancer patients who underwent surgery at Lanzhou University Second Hospital in 2022 and were used for Western blot analysis. Consent was obtained from the patients prior to the collection of all samples in this study. The experimental protocols were approved by the ethics committee of Lanzhou University Second Hospital and adhered to the tenets of the Declaration of Helsinki.

RNA Isolation and Quantitative Real-Time PCR

When the confluence of cells in each group reached 80%-90%, the cells were harvested, and total RNA was extracted using TRIzol RNA Isolation Reagent. The purity and concentration of RNA were determined by nanodrop. cDNA synthesis was performed using the FastKing cDNA first-strand Synthesis Kit from Tiangen, and further real-time quantitative PCR analysis was performed using the SuperReal PreMix Plus reagent and real-time PCR system (PikoReal 96, Thermo Fisher). All primers are listed in [Table S1](#), and GAPDH is the reference gene. The relative expression of genes was calculated using the $\Delta\Delta Ct$ algorithm.

Western Blot

Whole cell lysates from each group were obtained using RIPA lysates, and protein concentrations were determined using the BCA assay. Western blot was performed as described previously,¹⁷ RNF8/ γ H2A.X/ABCBI/ABCC1/ABCG2 antibodies were used to detect the target proteins, and GAPDH was used as an internal control to ensure equal sample loading. Finally, horseradish peroxidase-labeled secondary antibody was used to decompress the ECL liquid substrate, and the resulting fluorescence signal was detected by a chemiluminescence imaging system (MiniChemi, Sage Creation). Grayscale analysis of the bands was performed using ImageJ.

Immunohistochemistry

The tissue microarray was consisted of 48 pairs of paraffin-embedded colon cancer samples and corresponding adjacent normal tissues. After dewaxing and rehydration, antigen retrieval was performed with citrate buffer, followed by antigen blocking of tissue samples with PBS containing 10% goat serum for half an hour at 37°C. Samples were incubated overnight with primary antibody against RNF8. After washing, biotin-labeled goat anti-mouse secondary antibody and alkaline phosphatase-labeled streptavidin triple antibody were further added sequentially. Finally, the immune response was visualized using DAB and the images were acquired by scanning using pathological section scanner (HS6, Leica). Three of these pairs were not included in the statistics due to breakage and are identified by the red box in the [Figure S1E](#).

Preparation of FNAs

FNAs were synthesized according to the methods described in Christian Wiraja and Xiao's work.^{42,51} Four strands (a, b, c, and d) were mixed in equal proportions (20 μ L each strand) in 1 mL of TM buffer (10 mM Tris, 5 mM $MgCl_2$, pH = 8.0), heated to 95°C and cooled rapidly to 4°C to form Tet. While for si-Tet, the core tetrahedron with sticky end was first synthesized using the same method with four strands (a, b, c, and d with sticky end). The core part was then mixed with siRNF8 with sticky end at a ratio of 1:1, and the mixture was cooled at a rate of 0.1°C/min from 35°C to 20°C to form si-Tet, which was purified using a 30Kd ultrafiltration centrifuge tube by centrifuging at 14,000 g for 10 min. The sequences that assembled the FNAs were all listed in [Table S2](#).

FNAs and DOX were mixed in a certain proportion and incubated on a shaker at 80 rpm at 25°C for 1 h to load DOX into FNAs, and excess DOX was removed by ultrafiltration.

Characterization of FNAs

The obtained FNAs were analyzed by agarose gel electrophoresis and TEM. Briefly, FNAs, DOX-loaded FNAs, and the single strands composing FNAs were separately mixed with DNA loading buffer, and electrophoresis was carried out with 1.5% agarose gel at a constant voltage of 80 V for 80 min at 4°C. Finally, the images were acquired by the gel imaging system. For electron microscopy analysis, samples were dropped onto copper mesh coated with polyethylene formaldehyde support membrane and stained with 2% aqueous uranyl acetate, air-dried, and analyzed using electron microscopy (Tecnai F30, FEI). The zeta potential was measured using Zetasizer Nano (Malvern) following the manufacturer's guidelines. And the size distribution measurements of FNAs were conducted by dynamic light scattering (DLS) using a Zetasizer Nano (Malvern). Specifically, purified si-Tet as well as si-DOX-Tet were diluted using TM buffer to a final concentration of 1 μM . The mean hydrodynamic diameter of the two was determined via cumulative analysis. The DLS determinations were predicted based on the electrophoretic mobility of FNAs in aqueous medium. Electrophoretic mobility was assessed using a plastic sample cell in general mode and the measurements were repeated three times for each independent sample. The final average particle size is based on three independent replicates.

DOX Loading and Release Efficiency

The quantification of DOX was carried out by microplate reader (Synergy NEO2, Agilent). The absorbance at 480 nm of DOX at different concentrations (0, 15.625, 31.25, 62.5, 125, 250, 500, 1000, 2000 μM) was detected to establish the standard curve of concentration and absorbance value. To analyze the maximum drug loading of si-Tet, 200 μL of si-Tet (1 μM) were mixed with different volumes (1, 2, 5, 10, 20, and 50 μL) of DOX (1 mM) and incubated at 25°C for 1 h at 80 rpm on a shaker. For the groups with flocculent precipitates, the supernatant was collected as unloaded DOX by centrifugal centrifugation at 14,000 g for 10 min. The maximum DOX loading was further calculated by measuring the absorbance value of DOX at 480nm before and after incubation. For the analysis of DOX release efficiency, si-Tet was first loaded with the maximum amount of DOX and centrifuged to obtain the precipitate, and then the precipitate was resuspended in PBS at pH = 5.0 or pH = 7.4, respectively, and incubated at 37°C for 24 h. During this period, the supernatant was collected by centrifugation at the indicated time points (3, 6, 9, 12, and 24 h) and the absorbance value at 480 nm was measured. The precipitate was resuspended with the same volume of corresponding fresh PBS and the incubation continued. The cumulative release of DOX was analyzed based on the amount of DOX released at each time point.

Cellular Internalization of FNAs

To analysis cellular internalization of FNAs, cy3 was modified at the 5' end of b-strand to obtain cy3-labeled si-Tet (cy3-si-Tet). HCT116 cells were plated in 6-well plates and cy3-si-Tet was added to a final concentration of 5 nM. Cells were collected at different time points (0, 3, 8, 24 h), and the fluorescence intensity of cy3 in cells was detected by flow cytometry (NovoCyte Quanteon, Angilent) and fluorescence microscopy (BX43, Olympus), respectively. The escape of cy3-si-Tet and si-DOX-Tet from lysosomes after being internalized by the cell was further analyzed using fluorescence microscopy. Lyso-Tracker Green and Hoechst 33342 were added to label lysosomes and nuclei, respectively. Images were collected at 6, 12, and 24 hours by fluorescence microscopy (BX43, Olympus) and the subcellular localization of cy3-si-Tet was analyzed by ImageJ.

Intracellular DOX Measurement

Si-DOX-Tet and free DOX were separately added to the medium to analyze whether FNAs could facilitate DOX transport, and DOX was quantified as 1 μM . 12 h later, HCT116 cells were harvested for analysis of intracellular DOX fluorescence intensity by flow cytometry (NovoCyte Quanteon, Angilent), and untreated cells served as controls. The excitation and emission light of DOX used were 488 nm and 590 nm, respectively.

HCT116 cells were cultured in medium containing 50 nM of Tet or si-Tet for 48 h, respectively. DOX was added to a final concentration of 5 μM and incubated for 1 h, whereupon the medium was replaced with drug-free medium and incubated for an additional 1 h. The cells were harvested and the fluorescence intensity of DOX in the cells was determined by flow cytometry (NovoCyte Quanteon, Angilent).

Proliferation Assay

The detection of cell proliferation is carried out using the CCK-8 and according to the manufacturer's standard instructions. HCT116 cells were plated in 96-well plates with 100 μL of medium per well containing approximately 3000 cells. After 6 h, the medium was treated differently and incubated for 72 h. CCK-8 assay was performed every 12 h and the absorbance value at 450 nm was measured using a microplate reader (spark, TECAN).

Chemotherapy Sensitivity

The toxicity of different chemotherapeutic drugs to HCT116 cells and RKO cells was detected by CCK-8 assay. Cells were cultured in media containing Tet and si-Tet, respectively, referred to as the Tet group and the si-Tet group. Different concentrations of chemotherapeutic agents were added, and incubation continued for 72 hours. All wells were replaced with 100 μL of RPMI 1640 medium (containing 10 μL of CCK-8 reagent), incubated at 37°C for 1 h, and the absorbance value at 450nm was measured by microplate reader (spark, TECAN). The half maximal inhibitory concentration (IC_{50}) value was calculated to compare the sensitivity of the two groups of cells to chemotherapy drugs.

Flow Cytometry Detection of Cell Apoptosis

Cell apoptosis was detected by flow cytometry using Annexin V-PE/7-AAD apoptosis detection kit. HCT116 and RKO cells were first cultured in medium containing 50 nM of Tet or si-Tet, namely Tet group and si-Tet group. After 24 h, some of these cells were replaced with medium containing DOX-Tet or si-DOX-Tet to form DOX-Tet group and si-DOX-Tet group. Here, the concentration of DOX was normalized to 300 nM. The cells were incubated for a further 24 h, digested using trypsin without EDTA, and resuspended after collection by gentle centrifugation. Cells in each group were stained with Annexin V-PE/7-AAD in the dark for 15 min and then examined by the flow cytometry system (NovoCyte Quanteon, Angilent).

Statistical Analysis

All experimental data were from three independent replicates and were presented as mean \pm standard error (SEM). Student's *T*-test and two-way ANOVA were used to analyze the differences between groups, and $p < 0.05$ was considered statistically significant. GraphPad Prism 9 was used for statistical analysis and chart making. In all figures, * represents $p < 0.05$, whereas **, *** and **** represent $p < 0.01$, $p < 0.001$ and $p < 0.0001$, respectively.

Results

RNF8 Expression is Increased in Colon Cancer

With UALCAN,^{52,53} we retrieved the expression levels of RNF8 in colorectal cancer samples from the TCGA database, which included 41 normal colon tissues and 286 cases of colon cancer. Compared with normal colon tissues, RNF8 expression was elevated in colon cancer at all stages, irrespective of lymph node metastasis (Figure 1A, Figure S1A and Table S3). The TCGA also collected 10 rectal tissues and 166 rectal cancer samples. Transcriptome analysis revealed a similar expression profile, that is, RNF8 was also upregulated in rectal cancer (Figure S1B–D and Table S4). Next, we collected human normal colon epithelial cells (FHC) and human colon cancer cells (HCT116/RKO/SW480/SW620). Total RNA and whole cell lysates were extracted to analyze the expression of RNF8 in the colon cancer cell lines was analyzed using RT-PCR and Western blot, respectively. Compared to FHC, all four colon cancer cell lines expressed higher levels of RNF8 (Figure 1B and C). We subsequently assessed the expression of RNF8 in 10 pairs of colon cancer and corresponding adjacent tissues by Western blot analysis and obtained consistent results (Figure 1D and E). Furthermore, immunohistochemical analysis of RNF8 expression patterns in 45 pairs of colon cancer tissues and adjacent tissues yielded consistent results (Figure 1F and Figure S1E). We finally analyzed the impact of abnormally elevated RNF8 on the survival of CRC patients. Notably, CRC patients with high RNF8 expression had a poorer prognosis, suggesting that RNF8 inhibition may prolong the survival of CRC patients (Figure 1G). Overall, RNF8 was abnormally highly expressed in colon cancer.

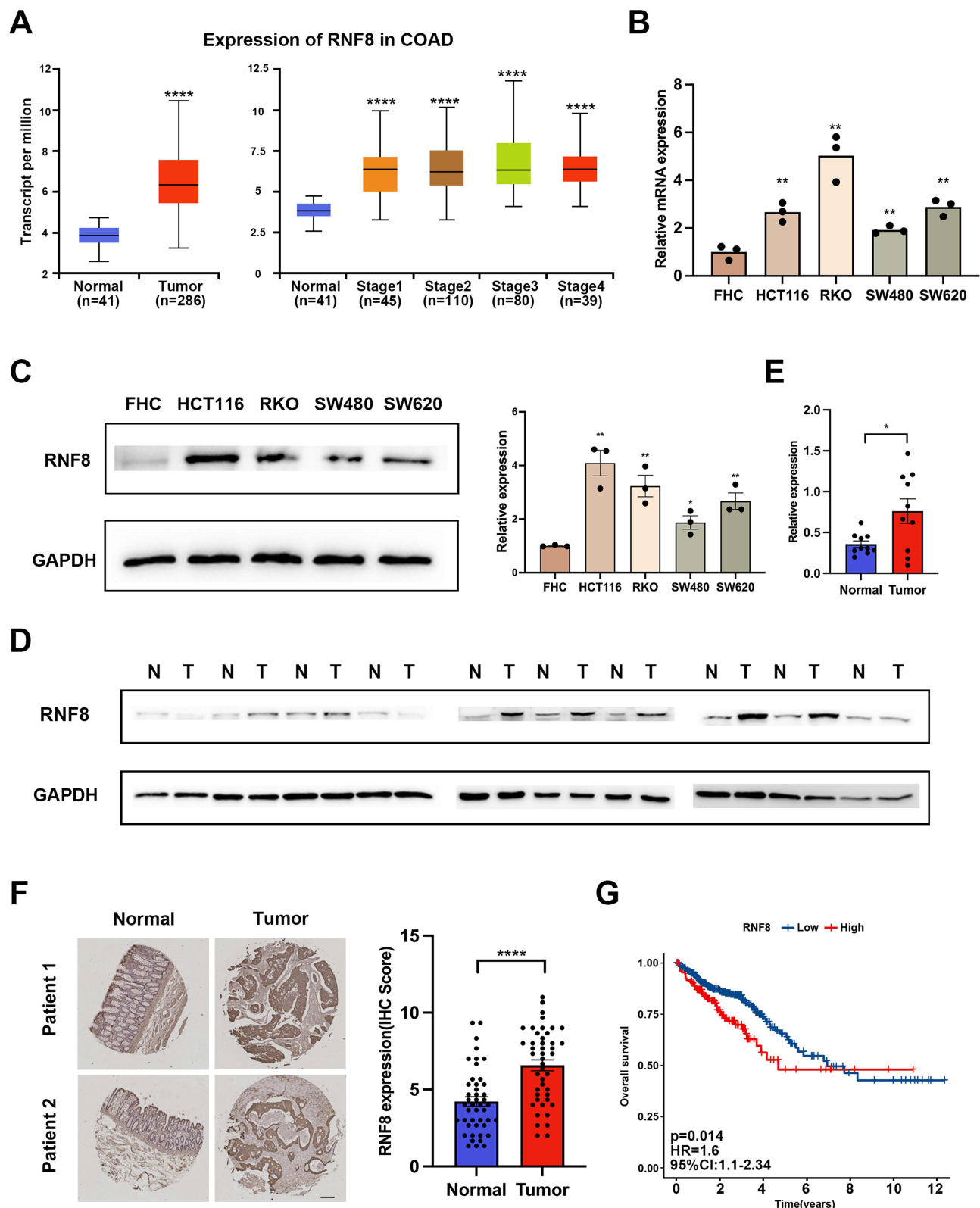


Figure 1 RNF8 is overexpressed in colon cancer. **(A)** Expression levels of RNF8 in colon cancer samples and normal samples in TCGA database based on sample type or tumor stage, respectively. **(B)** The expression of RNF8 in normal colonic epithelial cell FHC and four colon cancer cell lines was analyzed by RT-PCR. **(C)** Western blot analysis of RNF8 expression in the above five cell lines. **(D and E)** The expression levels of RNF8 in colon cancer samples and adjacent tissues were analyzed by Western blot (N: Normal T: Tumor). **(F)** Immunohistochemical analysis and representative images of 45 pairs of colon cancer samples and corresponding adjacent tissues, performed using anti-RNF8 antibodies and re-stained with hematoxylin. **(G)** Kaplan-Meier survival analysis showed that colon cancer patients with high RNF8 expression had a worse prognosis than those with low RNF8 expression. Data were obtained from The Human Protein Atlas (<https://www.proteinatlas.org/>). * represents $p < 0.05$, whereas ** and **** represent $p < 0.01$ and $p < 0.0001$, respectively.

Preparation of Tetrahedral FNAs

By mixing the four pre-designed DNA single strands in equal proportions, we first obtained DNA tetrahedra (Figure 2A and S2A). To suppress RNF8 expression level in colon cancer, we designed and generated siRNF8-loaded FNA based on Tet. The basic tetrahedral core is composed of four single-stranded DNA strands (a, b, c, and d with sticky end). And siRNF8 is connected to the tetrahedral core through complementary pairing of its sticky end with the sticky end of d (Figure 2A). Due to the malleability of DNA sequences, for tracing, cy3-labeled b-strands were used to assemble to form cy3-labeled DNA tetrahedron when necessary. Alternatively, DOX can easily intercalate into double-stranded DNA to form DOX-loaded FNAs (Figure 2A and B). Based on this, we intend to investigate the combined treatment of gene silencing and chemotherapy using nanoparticles.

Characterization of Tetrahedral FNAs

For the obtained si-Tet, after purification, they were firstly characterized by gel electrophoresis, and the tetrahedral and siRNF8 fractions that make up the FNAs were shown in the upper panel of Figure 2C. Next, the size distribution of the nanoparticles, with an average particle size of 10.29 nm and zeta potential of -17.92 mV, was analyzed using a zeta potentiometer (Figure 2D). In addition, the synthesis of nanoparticles was also verified by TEM, and the size of the nanoparticles was relatively uniform, about 10 nm, as shown in the electron microscope photos (Figure 2E).

Subsequently, we loaded DOX into tetrahedral FNAs, and as seen by gel electrophoresis after DOX loading, the band traveled a smaller distance than in the unloaded case due to the increased molecular weight (Figure 2C and Figure S2B). However, with the increased DOX loading, the positive charge of DOX neutralized the negative charge of DNA, resulting in weakened charge repulsion, flocculent precipitation in the solution, and obvious tailing in electrophoresis. The precipitate obtained by centrifugation was the tetrahedral FNAs loaded with DOX, and the supernatant was the unloaded DOX (Figure 2B). Therefore, the difference between the total DOX and the unloaded DOX was the drug loading of DOX (Figure S2C). To determine the maximum drug loading capacity of si-Tet, we added different concentrations of DOX until the drug loading was constant, and about 1 M tetrahedral FNA could load 210.46 M DOX (Figure S2D and E). Next, the particle size distribution and zeta potential of the drug-loaded tetrahedral FNA were also analyzed. After drug loading, the average particle size was increased to about 37.29 nm, and the zeta potential was also neutralized to -6.15 mV (Figure 2D). These results were consistent with the deterioration of the stability of the system and the formation of precipitation. Finally, the synthesis of drug-loaded tetrahedral FNA was also verified by TEM (Figure 2E).

The stable loading of DOX by si-DOX-Tet in the circulation and timely release of DOX in an acidic environment of the tumor site are essential for the cytotoxicity of DOX. For this purpose, si-DOX-Tet was incubated in PBS at pH = 5.0 and pH = 7.4, respectively, and the release of DOX was observed after incubation for different times. When it comes to physiological environments, less than 10% of DOX was released after 24 hours, which is approximately 8.69%. In an environment with pH = 5.0, DOX was rapidly released from si-DOX-Tet, reaching approximately 36.46% at 6 hours, and ultimately nearly half of DOX was released at 24 hours (Figure 3A).

Cellular Internalization of FNAs

DNA FNAs are ideal drug delivery carriers due to their intrinsic biocompatibility. We first verified whether Tet had any effect on cell growth at concentrations ranging from 0 to 100 nM by CCK-8 assay. The results showed that Tet had good biological safety and had no effect on cell proliferation within the range of 100 nM (Figure S3A). We next use cy3-si-Tet to investigate its interaction with colon cancer cells. The internalization of cy3-si-Tet into HCT116 cells was detected by flow cytometry and fluorescence microscopy within 24 h after cy3-si-Tet treatment. As shown in the Figure 3B and Figure S3B, the cy3 fluorescence signal was barely observed in the cells at 3 h, and flow cytometry results also showed the same baseline fluorescence intensity at 3 h as in control cells. Obvious intracellular fluorescence signal was tested at 8 h and 24 h, especially at 24 h. The same results were verified by flow cytometry.

Endo/lysosome-mediated endocytosis plays an important role in the cellular uptake of nanoparticles. We used lysosome green probe to label lysosomes and further tracked the localization of si-Tet after its entry into the cell by fluorescence microscopy. Firstly, at 6 h, a clear cy3 fluorescence signal was visible on the cell membrane, whereas the cy3 fluorescence signal could be observed in the cytoplasm at 12 h. More importantly, its coincidence with green fluorescence suggested that si-Tet was

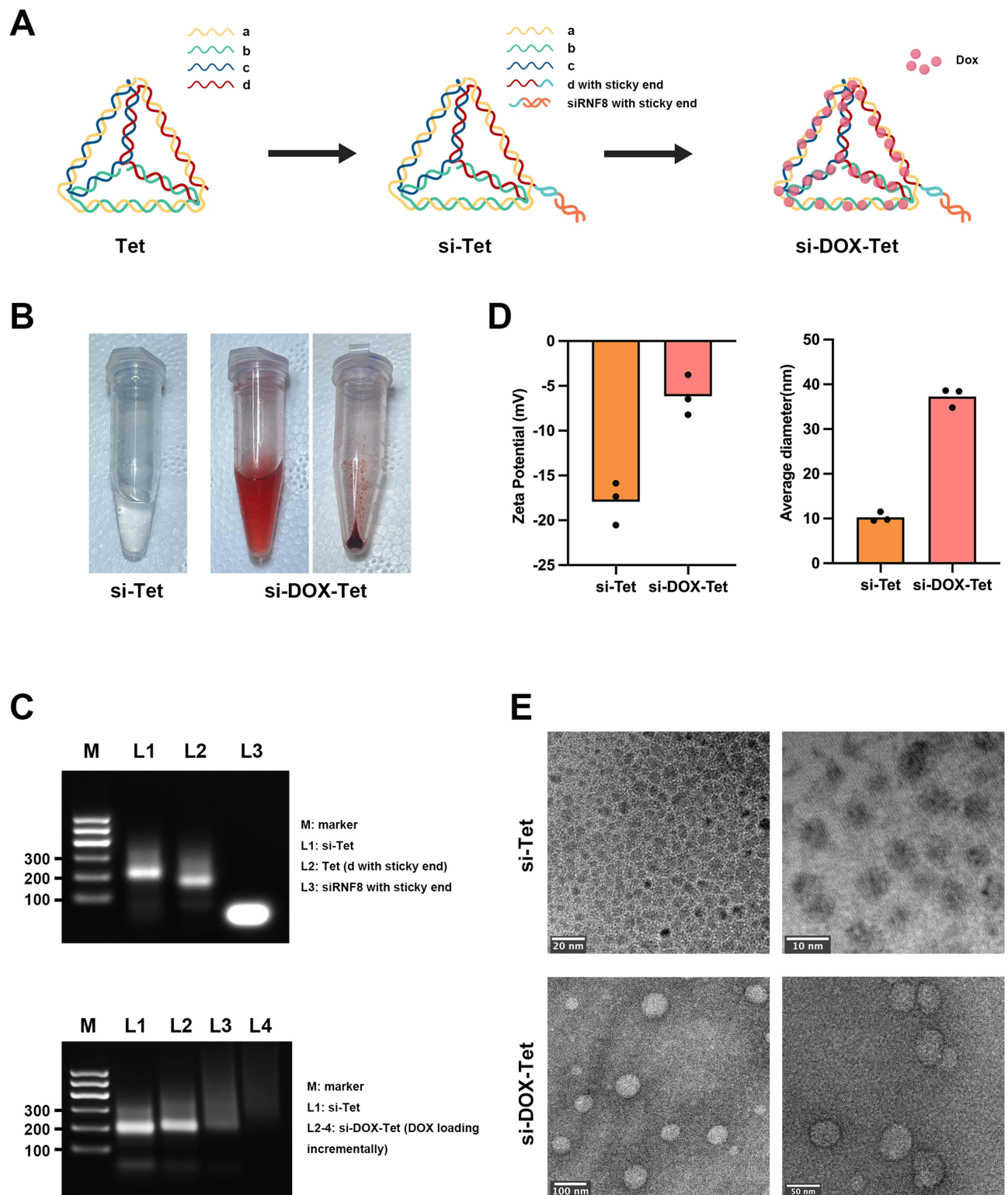


Figure 2 Characterization of tetrahedral FNAs. **(A)** Schematic diagram of tetrahedral FNAs synthesis. And a, b, c, and d in the figure represent the four single strands used to assemble the DNA tetrahedron. **(B)** Picture of si-Tet and si-DOX-Tet. The precipitate in the figure is si-DOX-Tet obtained by centrifugation after loading DOX of maximum drug loading capacity. **(C)** Agarose gel electrophoresis of tetrahedral FNAs. The image above shows si-Tet, tetrahedral part, and siRNase8 part; The figure below shows si-Tet and si-DOX-Tet with different loads of DOX. **(D)** Zeta potentials and particle size distribution analysis of si-Tet and si-DOX-Tet. **(E)** Transmission electron microscopy photos of si-Tet and si-DOX-Tet at different magnifications.

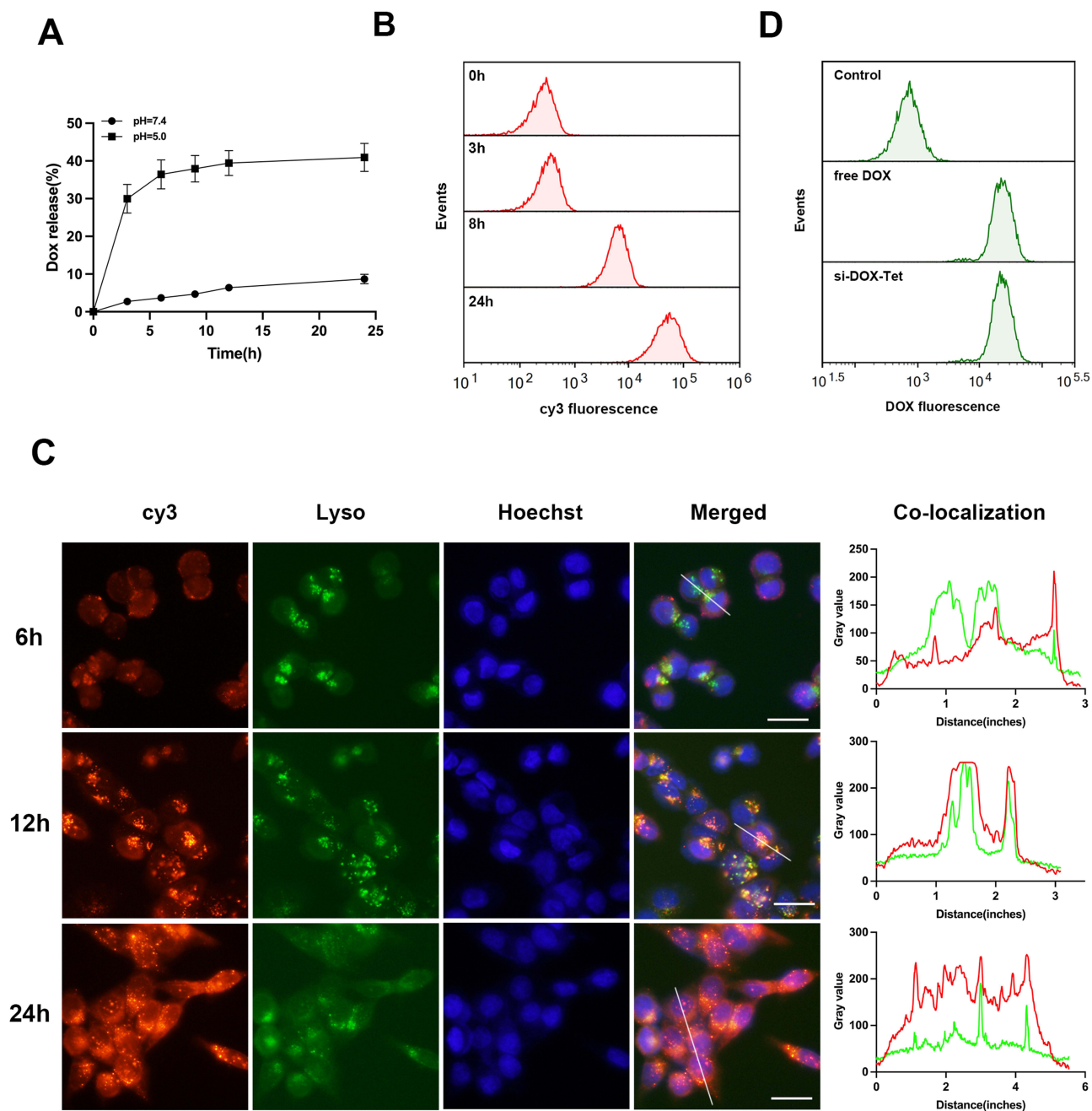


Figure 3 Cellular internalization of si-Tet. **(A)** The curve of DOX release from si-DOX-Tet incubated in PBS buffer of different pH values. **(B)** HCT116 cells were incubated with cy3-si-Tet for different times, and the fluorescence signal intensity of cy3 was analyzed by flow cytometry. **(C)** HCT116 cells were treated with cy3-si-Tet for different times. The subcellular localization of si-Tet was analyzed by fluorescence microscope, and Lysosome was labeled with Lyso-Tracker Green. Scale bar = 20 μ m. **(D)** HCT116 cells were treated with free DOX or si-DOX-Tet for 12 hours, and the efficiency of tetrahedral FNA transport of DOX was analyzed by flow cytometry.

successfully internalized into the cell and localized to lysosomes. Moreover, the cy3 fluorescence signal filled the cytoplasm at 24 hours, and the green fluorescence signal of the lysosome probe was also significantly reduced, suggesting that si-Tet successfully escape from the lysosome, which is crucial for the gene silencing effect (Figure 3C). DOX exerts its anti-cancer effect mainly via entering the nucleus and inserting between bases, affecting gene replication and causing DNA DSBs. Twenty-four hours after the addition of si-DOX-Tet, we also observed the successful entry of DOX into the nucleus (Figure S4A). To investigate whether si-Tet could facilitate DOX entry into cells, we incubated the cells with 1 μ M DOX or 100 nM drug-loaded tetrahedra (containing 1 μ M DOX) respectively. After 12 hours, significant DOX fluorescence signals were detected in both groups by flow cytometry

with no remarkable difference (Figure 3D). In conclusion, our synthesized FNAs were successfully internalized into cells in vitro and, more importantly, escaped from lysosomes, thus playing the role of gene silencing and chemotherapy.

Evaluation of the Efficiency of Silencing of RNF8 by Si-Tet

Interestingly, by flow cytometry, obvious cy3 fluorescence signal was observed in almost all cells (Figure S4B), manifesting the tetrahedron FNA can be used as efficient delivery carrier. Next, we investigated whether si-Tet could effectively silence RNF8 gene expression in HCT116. After 48 hours of incubation with 50 nM Tet, there was no effect on RNF8 expression compared with control cells. However, the level of RNF8 was significantly inhibited by si-Tet at 50 nM. More pronounced RNF8 inhibition was observed after adding more si-Tet (100 nM) (Figure 4A). Consistent results were also observed in RKO cells (Figure 4B). Similarly, Tet had no significant effect on the proliferation of HCT116 cells, whereas si-Tet could interrupt cell proliferation (Figure 4C). Based on this, we continued to test the effect of drug loaded tetrahedra FNAs on cell proliferation. As expected, after drug loading, HCT116 cell proliferation was significantly inhibited compared with the Tet group, while the si-DOX-Tet group exhibited stronger tumor inhibition (Figure 4D).

Si-Tet Mediated Inhibition of RNF8 Increases Chemotherapy Sensitivity of Colon Cancer Cells

To determine whether RNF8 inhibition increases the sensitivity of colon cancer cells to chemotherapeutic drugs, the IC_{50} of DOX to colon cancer cells was analyzed by CCK-8 assay. The results showed that the addition of si-Tet led to a nearly 2.5-fold decrease in the IC_{50} of DOX to colon cancer cells compared with the Tet group, which was 100.7 nM, while the latter was 261.2 nM. We further tested two other chemotherapy drugs, oxaliplatin and 5-FU, which represent widely used chemotherapeutic agents in numerous cancers. Inhibition of RNF8 resulted in a significant reduction in IC_{50} of oxaliplatin to HCT116 from 5.96 μ M to 1.27 μ M, while for 5-Fu, si-Tet also resulted in a significant reduction in IC_{50} of HCT116 (Figure 4E and Figure S5). The above results indicated that RNF8 expression inhibition in HCT116 increases its sensitivity to the three chemotherapeutic agents. Furthermore, consistent results were also observed in RKO cells, treatment of si-Tet also leads to an increase in the sensitivity of RKO cells to three chemotherapy drugs (Figure 4F and Figure S5). In summary, si-Tet can effectively inhibit the expression of RNF8, impair cell growth in colon cancer cells, and increase sensitivity to chemotherapy drugs.

Si-DOX-Tet Treatment Induced Significant DNA Damage and Apoptosis in Colon Cancer Cells

Considering the genomic toxicity of DOX and the important role of RNF8 in DNA damage repair, we further evaluated the DNA damage in cells after RNF8 inhibition by examining the expression level of γ H2A.X. si-Tet treatment resulted in increased γ H2A.X levels in HCT116 and RKO cells compared with Tet treatment. More interestingly, after 24 hours of si-DOX-Tet treatment, significantly higher γ H2A.X levels were detected in both HCT116 and RKO cells compared with DOX-Tet treatment, suggesting that si-DOX-Tet treatment caused more unrepaired DNA DSBs (Figure 5A and B). Accumulated unrepaired DNA damage can lead to apoptosis, which is crucial for inhibiting tumor proliferation by chemotherapy drugs. To verify si-Tet-induced RNF8 expression reduction could give rise to tumor cell apoptosis, we subsequently analyzed cell apoptosis using flow cytometry. After co-incubation of HCT116 cells with Tet or si-Tet, we detected the apoptosis level of each group of cells using flow cytometry. The results showed that inhibition of RNF8 led to an increase in cell apoptosis, and DOX treatment also caused partial cell apoptosis. More importantly, gene silencing of RNF8 combined with DOX treatment led to one-third of cell apoptosis (Figure 5C). Similar results were also verified with RKO cells, and the combination therapy significantly increased cell apoptosis (Figure 5D). Overall, si-DOX-Tet-mediated combination treatment resulted in more DNA DSBs and apoptosis.

RNF8 Silencing Resulted in the Inhibition of ABCG2 as Well as Intracellular DOX Accumulation

It is worth noting that after DOX treatment, we detected stronger DOX signals in the cells of the si-Tet group through flow cytometry (Figure 6A), indicating that inhibition of RNF8 caused more DOX to accumulate in the cells. ATP-binding cassette (ABC) transporters actively expel chemotherapeutic drugs out of the cell after decomposing ATP to

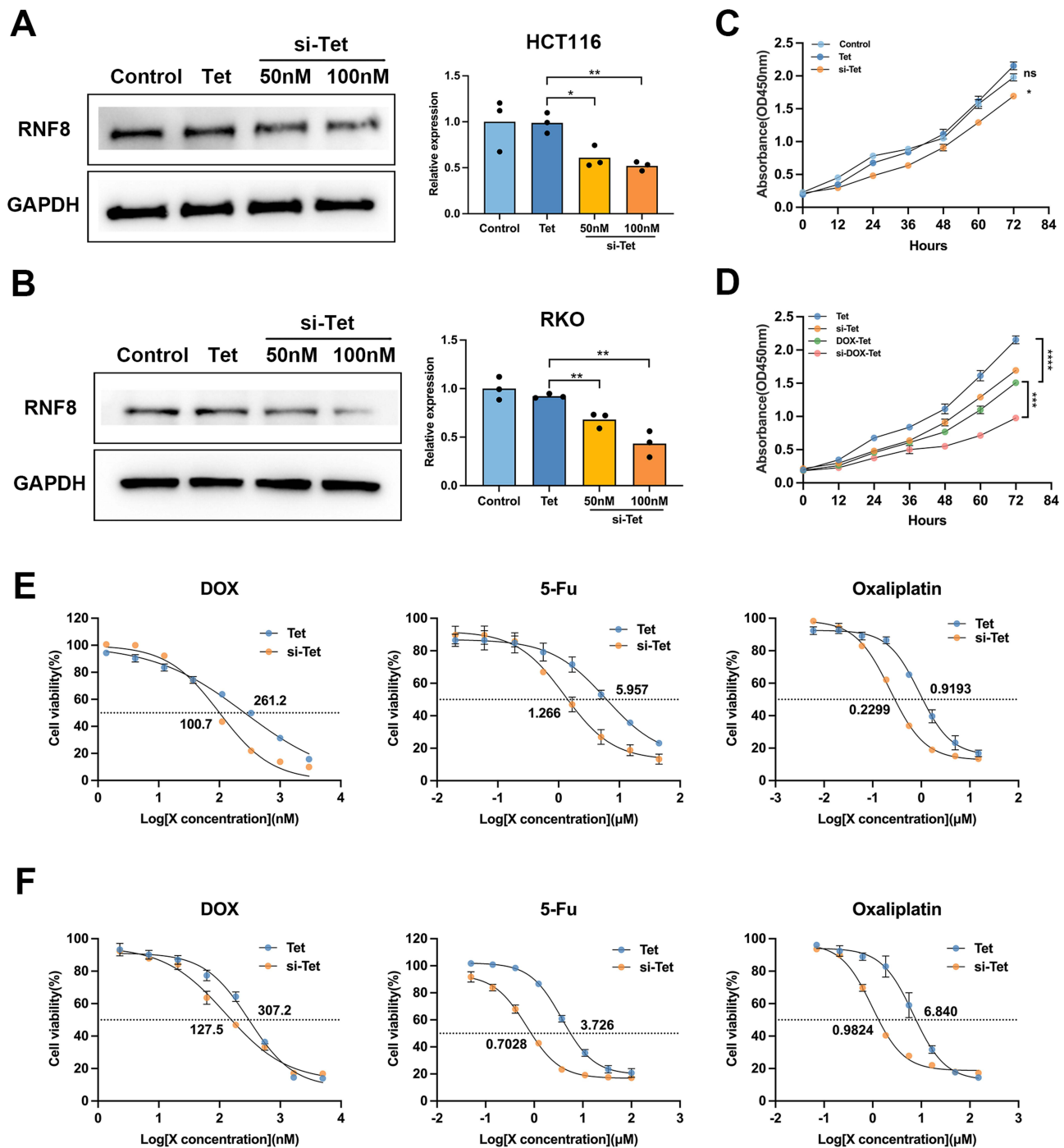


Figure 4 Effective Silencing of RNF8 by si-Tet. **(A)** HCT116 cells were treated with Tet, 50 or 100nM si-Tet, and RNF8 expression levels were analyzed by Western blot. **(B)** The silencing efficiency of RNF8 by si-Tet was determined by Western blot in RKO cells. **(C)** The proliferation of cells was evaluated using the CCK-8 assay. The concentration of both Tet and si-Tet was 50nM. **(D)** Analysis of proliferation of HCT116 cells with different treatments. The concentrations of DOX loaded to Tet and si-Tet are both 200 nM. **(E and F)** CCK-8 method was used to calculate the IC₅₀ of three chemotherapeutic drugs to colon cancer cells. The E panel shows HCT116 cells and the F refers to RKO cells. * represents p<0.05, whereas **, *** and **** represent p<0.01, p<0.001 and p<0.0001, respectively. ns = no significance.

obtain energy, weakening the efficacy of chemotherapy, and playing a crucial role in tumor drug resistance. We hypothesized that RNF8 inhibition might affect the expression or function of ATP-binding cassette (ABC) transporters, leading to increased intracellular DOX accumulation. To verify this, we tested three key factors in the ABC family, including ABCB1, ABCC1, and ABCG2. Total mRNA was extracted from the Tet and si-Tet groups, and RT-PCR analysis showed that the expression level of ABCG2 in the si-Tet group was significantly reduced, while ABCB1 and

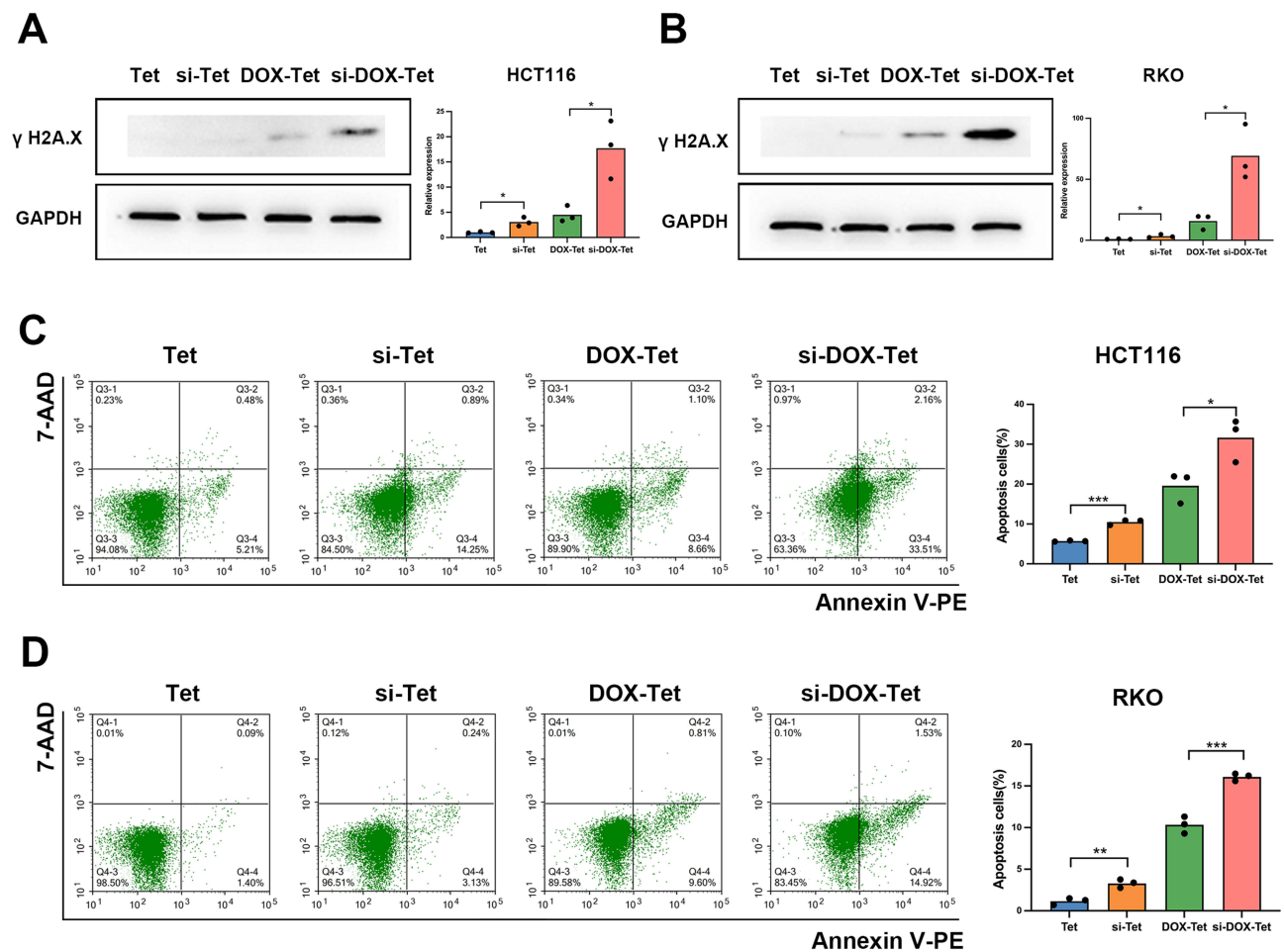


Figure 5 RNF8 inhibition induces apoptosis in colon cancer cells. **(A and B)** The DNA damage of HCT116 **(A)** and RKO **(B)** cells in each group was evaluated by detecting γ H2A.X expression by Western blot method. **(C)** The apoptosis ratio of HCT116 cells with different treatments was analyzed by flow cytometry. **(D)** Flow cytometry was used to detect the proportion of apoptotic RKO cells in each group. * represents $p < 0.05$, whereas ** and *** represent $p < 0.01$ and $p < 0.001$, respectively.

ABCC1 were not affected by RNF8 inhibition (Figure 6B). Further Western blot analysis also confirmed a decreased ABCG2 expression at the protein level (Figure 6C). Taken together, these results suggested that RNF8 inhibition causes a reduction in efflux of DOX by ABCG2, thereby increasing the therapeutic efficacy of DOX.

Discussion

Despite advancements in chemotherapy strategies for CRC, the low sensitivity to chemotherapy drugs and associated side effects continue to pose significant obstacles. Studies have reported that only a minority of patients benefit from adjuvant chemotherapy, exposing most patients to unnecessary toxicity.^{54,55} This implies that there is an urgent need to develop effective chemotherapy sensitization strategies to improve the survival and prognosis of CRC patients. In this study, the DNA tetrahedron was employed for the concurrent delivery of siRNF8 and DOX, resulting in a substantial enhancement of the chemotherapy efficacy of DOX via gene therapy, effectively suppressing the growth of colon cancer cells.

To date, numerous studies have indicated that the dysregulation of the RNF8 is linked to various types of tumors and is implicated in multiple tumor processes, including tumor proliferation, metastasis, and chemotherapy resistance.^{16,24–26} Firstly, RNF8 serves as a significant factor in DNA damage repair and plays a critical role in preserving genome stability through the regulation of DNA DSBs, which are the most detrimental form of genomic damage. RNF8-deficient mice are prone to developing lymphoma, thymoma, breast cancer, etc, suggesting that RNF8 is a tumor suppressor.^{16,22} Conversely, numerous studies have demonstrated that RNF8 may have a crucial role in the progression of tumors. By

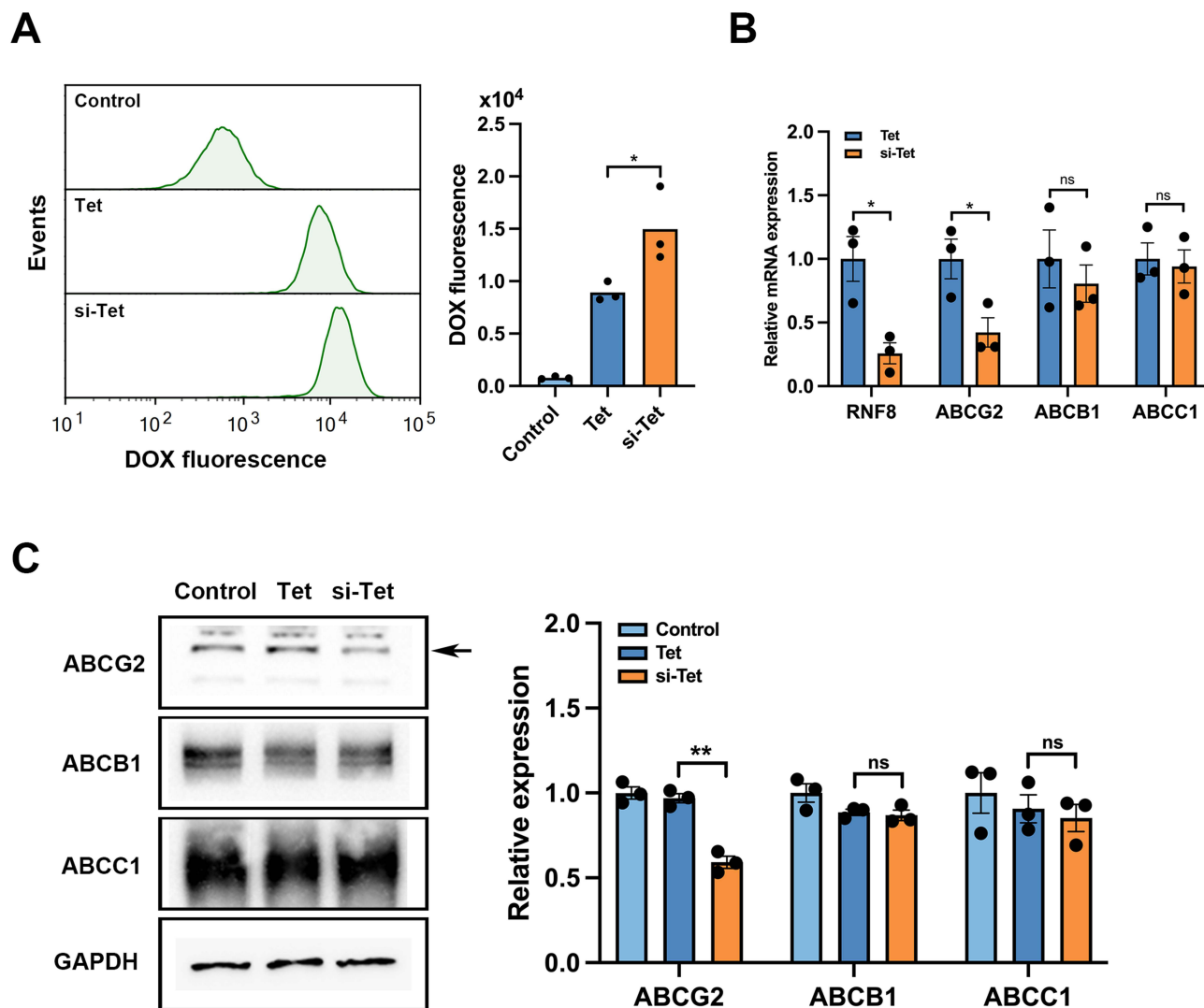


Figure 6 Inhibition of RNF8 leads to a decrease in DOX efflux in colon cancer cells. **(A)** The fluorescence intensity of DOX in the cells was measured by flow cytometry. **(B)** RT-PCR was used to detect the expression of key drug efflux genes caused by RNF8 silencing by si-Tet. **(C)** The expression changes of ABCB1, ABCC1, and ABCG2 were analyzed by Western blot. The arrow indicates the target bands. * represents $p < 0.05$, ** represents $p < 0.01$, ns = no significance.

analyzing colon cancer samples from TCGA database, clinical samples, and colon cancer cell lines, we identified that RNF8 was upregulated in different stages of colon cancer. And CRC patients with high RNF8 expression had a worse prognosis, aligning with the findings of Ren's work. They observed an upregulation of RNF8 expression and correlated with poor prognosis of colon cancer patients through immunohistochemical staining of 99 colon cancer samples and 78 benign samples. In addition, RNF8 has also been reported to promote chemotherapy resistance in breast and lung cancer, and in this study, inhibition of RNF8 mediated by si-DOX-Tet did promote colon cancer cell apoptosis induced by DOX treatment, increasing the chemotherapy sensitivity of DOX.^{27,28}

However, there is currently no research on increasing CRC chemotherapy sensitivity by inhibiting RNF8, particularly via the delivery of siRNF8 with nanocarriers. To suppress RNF8 in colon cancer, we designed and assembled si-Tet and si-DOX-Tet. The synthesis of both was characterized by gel electrophoresis, particle size and potential analysis, and TEM. Of utmost significance, the introduction of DOX did not alter the integrity of si-DOX-Tet. In addition, we also noticed that significant DOX release was detected under $pH = 5.0$ conditions, while in a neutral environment, DOX release from si-DOX-Tet was markedly slow. Mechanistically, DOX can intercalate into DNA through electrostatic attraction in a neutral environment, and the release of DOX from DNA FNAs depends on passive degradation in an acidic environment. In PBS buffer with $pH = 5.0$, the alteration in

surface charge of DNA FNAs and DOX weakens the electrostatic interaction, leading to the release of DOX from si-DOX-Tet. Ensuring consistent stability in the circulation or culture medium, while achieving controllable and efficient drug release in the acidic endosome/lysosomal environment of tumor targets, is essential for the successful delivery of drugs through nanocarriers.^{56,57} In general, si-DOX-Tet can serve as an effective DOX carrier for on-demand DOX loading and release. The raw materials of tetrahedral FNAs are deoxy-ribonucleoside triphosphates (dNTPs) and ribonucleoside triphosphates (NTPs). Therefore, addition of Tet at the highest concentration of 100 nM did not impact the viability of colon cancer cells. The simple design and synthesis, outstanding biocompatibility, and high drug loading capacity of DNA nanostructures render them as exceptional vehicles for the concurrent delivery of siRNA and DOX.

The cell membrane is negatively charged.^{58,59} As mentioned earlier, the negative charge carried by the phosphate group of DNA or RNA leads to electrostatic repulsion between the two, which is not favorable for the internalization of DNA FNAs into cells.⁵⁹ The loading of DOX may partially improve this situation. In fact, the size, shape, and base sequence of DNA FNAs are important factors that affect cellular uptake. DNA tetrahedron is transported to lysosome in a microtubule dependent manner through endocytosis.⁶⁰ Combining flow cytometry and fluorescence microscopy analysis, we noticed that after 6 hours of treatment with cy3-si-Tet or si-DOX-Tet, the tetrahedral FNA was mainly localized on the cell membrane. By 8 hours, a portion of the FNA could already be detected in the cytoplasm. After 12 hours, a large amount of DNA FNA and DOX were detected in the lysosome. In general, colon cancer cells showed a high uptake efficiency of tetrahedral FNA as they were detected in almost all cells. However, the acidic environment of lysosome will destroy the DNA FNAs. Only successfully escaping from lysosome can ensure the efficiency of gene silencing and the toxicity of DOX. Therefore, we continued to track cy3 and DOX, and at 24 hours, we observed cy3 signals spreading throughout the cytoplasm, as well as fluorescence signals of DOX in the nucleus. After 48 hours, we extracted whole cell lysate and observed significant inhibition of RNF8 expression levels. These results indicated that the tetrahedral FNA was successfully internalized into cells and effectively silenced genes. Further, we also observed that si-Tet mediated RNF8 deficiency resulted in proliferation inhibition of colon cancer cells, and the IC₅₀ of three chemotherapy drugs to colon cancer cells was reduced, indicating a notable enhancement in chemosensitivity.

In eukaryotic cells, DNA damage triggers the recruitment of multiple post-translational modification (PTM) factors as switches to regulate cell cycle, DNA repair, and apoptosis, known as DNA damage response (DDR).^{61,62} Upon the formation of DSBs, ataxia telangiectasia mutated/ataxia telangiectasia and RAD3-related protein (ATM/ATR) kinases are initially recruited to the damage sites and activated, thereby inducing phosphorylation of histone variant H2AX (γ H2A.X).^{62,63} It subsequently recruits DNA repair related proteins, including RNF8, to accumulate at the site of damage to facilitate the completion of DNA repair. γ H2A.X plays a crucial role in early DNA damage response and is widely regarded as the primary indicator for measuring DSB levels.^{64,65} RNF8 accumulates rapidly at the damaged sites during the repair and facilitates recruitment of repair proteins such as p53-binding protein 1 (53BP1) and breast cancer susceptibility protein 1 (BRCA1) to the damaged chromatin by regulating ubiquitination of histone H2A and H2AX, thus being indispensable for the repair process.^{61,62,66} In our prior study, we employed RNF8 knockout model mice and observed that RNF8 is essential for DNA damage repair in mouse neurons. The deficiency of RNF8 alone is adequate to induce neuronal pathology, resulting in neuronal degeneration.¹⁷ DOX inhibits Top2 by forming covalent Top2-DOX-DNA complex, leading to DSBs.⁶⁷ When DNA damage is severe and irreparable, it will induce cell apoptosis.⁶² The notably elevated levels of γ H2A.X and cell apoptosis following si-Tet and si-DOX-Tet treatment suggested elevated DNA damage, and RNF8 inhibition increased the sensitivity of DOX treatment.

Tumor cells have been found to develop various mechanisms to resist chemotherapy, with more than 100 genes identified as being linked to reduced sensitivity to tumor chemotherapy.⁶⁸ Among them, the ATP binding cassette (ABC) proteins superfamily is responsible for the elimination of chemotherapy drugs from the cells, especially ABCB1, ABCC1, and ABCG2.^{69–71} The substantial reduction in ABCG2 expression following RNF8 silencing is accountable for the notable elevation in intracellular DOX levels. Increased intracellular DOX induced the formation of more DNA damage. Xu et al reported that RNF8 expression is increased in lung cancer. In the context of DNA damage induced by DOX treatment, it can regulate Akt activation through K63-linked ubiquitination, promoting lung cancer cell survival and chemotherapy resistance. In our study, inhibition of RNF8 also leads to DNA damage repair defects caused by DOX. In general, after treatment with si-DOX-Tet, cell proliferation slowed down, and apoptosis increased significantly, si-DOX-Tet exhibited a significant and effective inhibitory effect on colon cancer. Nevertheless, further investigation is required to elucidate the precise mechanism through which RNF8 regulates ABCG2.

Conclusion

In summary, we constructed si-DOX-Tet based on the advantages of DNA FNAs and the fact that the expression of RNF8 is significantly increased in colon cancer. The nanocarrier facilitates the co-delivery of siRNF8 and DOX to colon cancer cells for collaborative therapy, achieving both drug delivery and increased drug efficacy. This DNA based nanocarrier can be precisely predesigned to carry a specific ratio of siRNF8 and DOX, with simple, controllable, and efficient synthesis. Studies on the interaction between cells and nanocarriers shown that si-DOX-Tet can be internalized into cells and escape smoothly from lysosomes, ensuring siRNF8 and DOX are delivered to the cytoplasm and nucleus, respectively. Subsequent in vitro investigations demonstrated that the overexpression of RNF8 in colon cancer cells could be effectively inhibited by si-Tet, thereby slowing down their proliferation and increasing sensitivity to chemotherapy drugs. si-DOX-Tet mediated gene suppression combined with chemotherapy can significantly induce DNA damage and apoptosis of colon cancer cells. Mechanistically, RNF8 inhibition leads to the inhibition of ABCG2 expression and reduces DOX efflux, thereby enhancing the chemotherapeutic efficacy of DOX. The DNA FNAs utilized in this study exhibit favorable biocompatibility, and the type and amount of siRNA and chemotherapy drugs loaded are precisely adjustable. Moreover, it can be designed to connect nucleic acid aptamers, DNA probes, and antisense nucleic acids to achieve a variety of functions. Overall, the si-DOX-Tet constructed in this study demonstrates the great potential of DNA FNAs in the precise and efficient treatment of tumors.

Abbreviations

CRC, Colorectal cancer; DOX, Doxorubicin; EMT, epithelial-mesenchymal transition; Tet, tetrahedron; TEM, Transmission electron microscope; FNA, Frame nucleic acid, DSBs, Double-strand breaks; ABC, ATP binding cassette.

Data Sharing Statement

All relevant data are included in the main manuscript and supplementary materials. Supporting/raw data are available from the corresponding author on reasonable request.

Funding

This work was supported by the National Natural Science Foundation of China (Grants No. 82071695 to Degui Wang and No. 82060535 to Yingxia Tian) and lzuyxcx-2022-155 from Medical Innovation and Development Project of Lanzhou University.

Disclosure

The authors declare no conflict of interest.

References

1. Ferlay J, Colombet M, Soerjomataram I, et al. Cancer statistics for the year 2020: an overview. *Inter J Can.* 2021;149:778–789. doi:10.1002/ijc.33588
2. Biller LH, Schrag D. Diagnosis and treatment of metastatic colorectal cancer: a review. *JAMA.* 2021;325:669–685. doi:10.1001/jama.2021.0106
3. Khan FAO, Albalawi R, Pottoo FH. Trends in targeted delivery of nanomaterials in colon cancer diagnosis and treatment. *Med Res Rev.* 2022;42(1):227–258. doi:10.1002/med.21809
4. Li P, Zhang X, Wang H, et al. MALAT1 is associated with poor response to oxaliplatin-based chemotherapy in colorectal cancer patients and promotes chemoresistance through EZH2. *Mol Cancer Ther.* 2017;16:739–751. doi:10.1158/1535-7163.MCT-16-0591
5. Zhu C, Zhang L, Zhao S, Dai W, Xu Y. UPF1 promotes chemoresistance to oxaliplatin through regulation of TOP2A activity and maintenance of stemness in colorectal cancer. *Cell Death Dis.* 2021;12(6):519. doi:10.1038/s41419-021-03798-2
6. Kalyanaraman B. Teaching the basics of the mechanism of doxorubicin-induced cardiotoxicity: have we been barking up the wrong tree? *Redox Biol.* 2020;29:101394. doi:10.1016/j.redox.2019.101394
7. Renu K, Vg A, P.b TP, Arunachalam S. Molecular mechanism of doxorubicin-induced cardiomyopathy – an update. *Eur J Pharmacol.* 2018;818:241–253. doi:10.1016/j.ejphar.2017.10.043
8. Rawat PS, Jaiswal A, Khurana A, Bhatti JS, Navik U. Doxorubicin-induced cardiotoxicity: an update on the molecular mechanism and novel therapeutic strategies for effective management. *Biomed Pharmacother.* 2021;139:111708. doi:10.1016/j.biopha.2021.111708
9. Alibolandi M, Abnous K, Mohammadi M, et al. Extensive preclinical investigation of polymersomal formulation of doxorubicin versus Doxil-mimic formulation. *J Control Release.* 2017;264:228–236. doi:10.1016/j.jconrel.2017.08.030
10. Russell LM, Hultz M, Searson PC. Leakage kinetics of the liposomal chemotherapeutic agent Doxil: the role of dissolution, protonation, and passive transport, and implications for mechanism of action. *J Control Release.* 2018;269:171–176. doi:10.1016/j.jconrel.2017.11.007

11. Hosseini NF, Amini R, Ramezani M, et al. AS1411 aptamer-functionalized exosomes in the targeted delivery of doxorubicin in fighting colorectal cancer. *Biomed Pharmacother.* 2022;155:113690. doi:10.1016/j.biopha.2022.113690
12. Christidi E, Brunham LA-O. Regulated cell death pathways in doxorubicin-induced cardiotoxicity. *Cell Death Dis.* 2021;12(4):339. doi:10.1038/s41419-021-03614-x
13. Wu L, Wang L, Du Y, Zhang Y, Ren J. Mitochondrial quality control mechanisms as therapeutic targets in doxorubicin-induced cardiotoxicity. *Trends Pharmacol Sci.* 2023;44:34–49. doi:10.1016/j.tips.2022.10.003
14. Guo Z, Tian Y, Guo Y, et al. RAD6B plays a critical role in neuronal DNA damage response to resist neurodegeneration. *Front Cell Neurosci.* 2019;13:392. doi:10.3389/fncel.2019.00392
15. Guo Y, Song Y, Guo Z, et al. Function of RAD6B and RNF8 in spermatogenesis. *Cell Cycle.* 2018;17:162–173. doi:10.1080/15384101.2017.1361066
16. Zhou T, Yi F, Wang Z, et al. The Functions of DNA Damage Factor RNF8 in the pathogenesis and progression of cancer. *Int J Bio Sci.* 2019;15(5):909. doi:10.7150/ijbs.31972
17. Ouyang S, Song Y, Tian Y, et al. RNF8 deficiency results in neurodegeneration in mice. *Neurobiol Aging.* 2015;36:2850–2860. doi:10.1016/j.neurobiolaging.2015.07.010
18. Tracz MA-O, Bialek WA-O. Beyond K48 and K63: non-canonical protein ubiquitination. *Cell Mol Biol Lett.* 2021;26(1):1. doi:10.1186/s11658-020-00245-6
19. Martínez-Férriz A, Ferrando A, Fathinajafabadi A, Farràs R. Ubiquitin-mediated mechanisms of translational control. *Semin Cell Dev Biol.* 2022;132:146–154. doi:10.1016/j.semcdb.2021.12.009
20. Kolla S, Ye M, Mark KG, Rapé M. Assembly and function of branched ubiquitin chains. *Trends Biochem Sci.* 2022;2022:1.
21. Cao L, Liu X, Zheng B, Xing CA-OX, Liu JA-O. Role of K63-linked ubiquitination in cancer. *Cell Death Discovery.* 2022;8(1):410. doi:10.1038/s41420-022-01204-0
22. Li L, Halaby M-J, Hakem A, et al. Rnf8 deficiency impairs class switch recombination, spermatogenesis, and genomic integrity and predisposes for cancer. *J Exp Med.* 2010;207(5):983–997. doi:10.1084/jem.20092437
23. Ren L, Zhou T, Wang Y, et al. RNF8 induces β -catenin-mediated c-Myc expression and promotes colon cancer proliferation. *Int J Bio Sci.* 2020;16(12):2051. doi:10.7150/ijbs.44119
24. Kuang J, Min L, Liu C, Chen S, Zhu L. RNF8 promotes epithelial-mesenchymal transition in lung cancer cells via stabilization of slug. *Mol Cancer Res.* 2020;1211:2019.
25. Kuang J, Li L, Guo L, et al. RNF8 promotes epithelial-mesenchymal transition of breast cancer cells. *J Exp Clin Cancer Res.* 2016;35(1):1–4. doi:10.1186/s13046-016-0363-6
26. Zhou T, Wang S, Song X, et al. RNF8 up-regulates AR/ARV7 action to contribute to advanced prostate cancer progression. *Cell Death Dis.* 2022;13(4):352. doi:10.1038/s41419-022-04787-9
27. Xu Y, Hu Y, Xu T, et al. RNF8-mediated regulation of Akt promotes lung cancer cell survival and resistance to DNA damage. *Cell Rep.* 2021;37:109854. doi:10.1016/j.celrep.2021.109854
28. Lee HJ, Li C-F, Ruan D, et al. The DNA damage transducer RNF8 facilitates cancer chemoresistance and progression through twist activation. *Molecular Cell.* 2016;63(6):1021–1033. doi:10.1016/j.molcel.2016.08.009
29. Gogoi P, Kaur G, Singh NK. Nanotechnology for colorectal cancer detection and treatment. *World J Gastroenterol.* 2022;28(46):6497. doi:10.3748/wjg.v28.i46.6497
30. Kasi PB, Mallela VR, Ambrozkiwicz F, et al. Theranostics nanomedicine applications for colorectal cancer and metastasis: recent advances. *Int J Mol Sci.* 2023;24(9):7922. doi:10.3390/ijms24097922
31. Haggag Y, Elshikh M, El-Tanani M, et al. Nanoencapsulation of sophorolipids in PEGylated poly(lactide-co-glycolide) as a novel approach to target colon carcinoma in the murine model. *Drug Delivery Transl Res.* 2020;10:1353–1366. doi:10.1007/s13346-020-00750-3
32. Ibrahim B, Mady OY, Tambuwala MM, Haggag YA. pH-sensitive nanoparticles containing 5-fluorouracil and leucovorin as an improved anti-cancer option for colon cancer. *Nanomedicine.* 2022;17:367–381. doi:10.2217/nnm-2021-0423
33. Pavitra E, Dariya B, Srivani G, et al. Engineered nanoparticles for imaging and drug delivery in colorectal cancer. *Semi Cancer Biol.* 2021;69:293–306. doi:10.1016/j.semcancer.2019.06.017
34. Younis NK, Roumieh R, Bassil EP, et al. Nanoparticles: attractive tools to treat colorectal cancer. *Semi Cancer Biol.* 2022;86:1–13. doi:10.1016/j.semcancer.2022.08.006
35. Naeimi R, Najafi R, Molaei P, Amini R, Pecic S. Nanoparticles: the future of effective diagnosis and treatment of colorectal cancer? *Eur J Pharmacol.* 2022;936:175350. doi:10.1016/j.ejphar.2022.175350
36. Rothemund PW. Folding DNA to create nanoscale shapes and patterns. *Nature.* 2006;440(7082):297–302. doi:10.1038/nature04586
37. Udomprasert A, Kangsamaksin TA-O. DNA origami applications in cancer therapy. *Cancer Sci.* 2017;108(8):1535–1543. doi:10.1111/cas.13290
38. Hong F, Zhang F, Liu Y, Yan HA-O. DNA origami: scaffolds for creating higher order structures. *Chem. Rev.* 2017;117(20):12584–12640. doi:10.1021/acs.chemrev.6b00825
39. Zeng Y, Nixon RL, Liu W, Wang R. The applications of functionalized DNA nanostructures in bioimaging and cancer therapy. *Biomaterials.* 2021;268:120560. doi:10.1016/j.biomaterials.2020.120560
40. Ji JA-O, Karna DA-O, Mao HA-O. DNA origami nano-mechanics. *Chem Soc Rev.* 2021;50(21):11966–11978. doi:10.1039/D1CS00250C
41. Jiang Q, Liu S, Liu J, Wang ZG, Ding BA-O. Rationally designed DNA-origami nanomaterials for drug delivery in vivo. *Adv Mater.* 2019;31(45):1804785. doi:10.1002/adma.201804785
42. Wiraja C, Zhu Y, Lio DCS, et al. Framework nucleic acids as programmable carrier for transdermal drug delivery. *Nat Commun.* 2019;10(1):1147. doi:10.1038/s41467-019-09029-9
43. Ouyang X, Wu Y, Guo L, et al. Self-assembly induced enhanced electrochemiluminescence of copper nanoclusters using DNA nanoribbon templates. *Angew Chem Int.* 2023;62(21):e202300893. doi:10.1002/anie.202300893
44. Ouyang XA-O, Wang S-Y, Liu T, et al. Functional modulation of cytochrome C upon specific binding to DNA nanoribbons. *Chem. Commun.* 2019;55(93):14074–14077. doi:10.1039/C9CC05427H
45. Linko V, Ora A, Kostiaainen MA. DNA nanostructures as smart drug-delivery vehicles and molecular devices. *Trends Biotechnol.* 2015;33:586–594. doi:10.1016/j.tibtech.2015.08.001

46. Jorge AF, Aviñó A, Pais AA, Eritja R, Fàbrega C. Fàbrega C DNA-based nanoscaffolds as vehicles for 5-fluoro-2'-deoxyuridine oligomers in colorectal cancer therapy. *Nanoscale*. 2018;10(15):7238–7249. doi:10.1039/C7NR08442K
47. Wang Z, Song L, Liu Q, et al. A tubular DNA Nanodevice as a siRNA/chemo-drug co-delivery vehicle for combined cancer therapy. *Angew Chem*. 2021;133(5):2626–2630. doi:10.1002/ange.202009842
48. Xu T, Yu S, Sun Y, et al. DNA origami frameworks enabled self-protective siRNA delivery for dual enhancement of chemo-photothermal combination therapy. *Small*. 2021;17(46):2101780. doi:10.1002/smll.202101780
49. Pan QA-O, Nie C, Hu Y, et al. Aptamer-functionalized DNA origami for targeted codelivery of antisense oligonucleotides and doxorubicin to enhance therapy in drug-resistant cancer cells. *ACS Appl Mater Interfaces*. 2019;12(1):400–409. doi:10.1021/acsami.9b20707
50. Liu J, Song L, Liu S, et al. A Tailored DNA nanoplatform for synergistic RNAi-/chemotherapy of multidrug-resistant tumors. *Angew Chem Int*. 2018;57:15486–15490. doi:10.1002/anie.201809452
51. Xiao D, Li Y, Tian T, et al. Tetrahedral framework nucleic acids loaded with aptamer AS1411 for siRNA delivery and gene silencing in malignant melanoma. *ACS Appl Mater Interfaces*. 2021;13:6109–6118. doi:10.1021/acsami.0c23005
52. Chandrashekar DS, Bachel B, Balasubramanya SAH, et al. UALCAN: a portal for facilitating tumor subgroup gene expression and survival analyses. *Neoplasia*. 2017;19(8):649–658. doi:10.1016/j.neo.2017.05.002
53. Chandrashekar DS, Karthikeyan SK, Korla PK, et al. UALCAN: an update to the integrated cancer data analysis platform. *Neoplasia*. 2022;25:18–27. doi:10.1016/j.neo.2022.01.001
54. Ghosh S, Singh R, Vanwinkle ZM, et al. Microbial metabolite restricts 5-fluorouracil-resistant colonic tumor progression by sensitizing drug transporters via regulation of FOXO3-FOXM1 axis. *Theranostics*. 2022;12(12):5574. doi:10.7150/thno.70754
55. Wang H, Yang W, Qin Q, et al. E3 ubiquitin ligase MAGI3 degrades c-Myc and acts as a predictor for chemotherapy response in colorectal cancer. *Mol Cancer*. 2022;21(1):1–9. doi:10.1186/s12943-022-01622-9
56. Zeng Y, Liu J, Yang S, et al. Time-lapse live cell imaging to monitor doxorubicin release from DNA origami nanostructures. *J Mat Chem B*. 2018;6(11):1605–1612. doi:10.1039/C7TB03223D
57. Li M, Yang G, Zheng Y, et al. NIR/pH-triggered aptamer-functionalized DNA origami nanovehicle for imaging-guided chemo-phototherapy. *J Nanobiotechnol*. 2023;21(1):186. doi:10.1186/s12951-023-01953-9
58. Zhang H, Wei X, Liu L, Zhang Q, Jiang W. The role of positively charged sites in the interaction between model cell membranes and γ -Fe(2)O(3) NPs. *Sci Total Environ*. 2019;673:414–423. doi:10.1016/j.scitotenv.2019.04.074
59. Xie S, Sun W, Fu T, et al. Aptamer-based targeted delivery of functional nucleic acids. *J Am Chem Soc*. 2023;145:7677–7691. doi:10.1021/jacs.3c00841
60. Fao S, Zeshan M, Laraib U, et al. DNA based and stimuli-responsive smart nanocarrier for diagnosis and treatment of cancer: applications and challenges. *Cancers*. 2021;13(14):3396. doi:10.3390/cancers13143396
61. Huen MS, Grant R, Manke I, et al. RNF8 transduces the DNA-damage signal via histone ubiquitylation and checkpoint protein assembly. *Cell*. 2007;131(5):901–914. doi:10.1016/j.cell.2007.09.041
62. Deshar R, Yoo W, Cho EB, Kim S, Yoon JB. RNF8 mediates NONO degradation following UV-induced DNA damage to properly terminate ATR-Chk1 checkpoint signaling. *Nucleic Acids Res*. 2019;47(2):762–778. doi:10.1093/nar/gky1166
63. Sun J, Zhu Z, Li W, et al. UBE2T-regulated H2AX monoubiquitination induces hepatocellular carcinoma radioresistance by facilitating Chk1 activation. *J Exp Clin Cancer Res*. 2020;39(1):1–8. doi:10.1186/s13046-020-01734-4
64. Geißler DA-O, Wegmann M, Jochum T, et al. An automatable platform for genotoxicity testing of nanomaterials based on the fluorometric γ -H2AX assay reveals no genotoxicity of properly surface-shielded cadmium-based quantum dots. *Nanoscale*. 2019;11(28):13458–13468. doi:10.1039/C9NR01021A
65. Zhang B, Li F, Shen L, et al. A cathodic photoelectrochemical immunoassay with dual signal amplification for the ultrasensitive detection of DNA damage biomarkers. *Biosens Bioelectron*. 2023;224:115052. doi:10.1016/j.bios.2022.115052
66. Li F, Liu B, Zhou X, Xu Q. Silencing of E3 ubiquitin ligase RNF8 enhances ionizing radiation sensitivity of medulloblastoma cells by promoting the deubiquitination of PCNA. *Oncology Res*. 2018;26(9):1365. doi:10.3727/096504018X15154085345907
67. Deng S, Yan T, Jendry C, et al. Dexrazoxane may prevent doxorubicin-induced DNA damage via depleting both topoisomerase II isoforms. *BMC Cancer*. 2014;14:1. doi:10.1186/1471-2407-14-842
68. Marin JA-O, Monte MJ, Macias RI, et al. Expression of chemoresistance-associated ABC proteins in hepatobiliary, pancreatic and gastrointestinal cancers. *Cancers*. 2022;14(14):3524.
69. Low FG, Shabir KAO, Brown JE, Rao B, Rothnie AJ. Roles of ABCC1 and ABCC4 in proliferation and migration of breast cancer cell lines. *Int J Mol Sci*. 2020;21(20):7664. doi:10.3390/ijms21207664
70. Ramos A, Sadeghi S, Tabatabaieian HAO. Battling chemoresistance in cancer: root causes and strategies to uproot them. *Int J Mol Sci*. 2021;22(17):9451. doi:10.3390/ijms22179451
71. Gao Q, Li -X-X, Xu Y-M, et al. IRE1 α -targeting downregulates ABC transporters and overcomes drug resistance of colon cancer cells. *Cancer Lett*. 2020;476:67–74. doi:10.1016/j.canlet.2020.02.007

International Journal of Nanomedicine

Dovepress

Publish your work in this journal

The International Journal of Nanomedicine is an international, peer-reviewed journal focusing on the application of nanotechnology in diagnostics, therapeutics, and drug delivery systems throughout the biomedical field. This journal is indexed on PubMed Central, MedLine, CAS, SciSearch®, Current Contents®/Clinical Medicine, Journal Citation Reports/Science Edition, EMBase, Scopus and the Elsevier Bibliographic databases. The manuscript management system is completely online and includes a very quick and fair peer-review system, which is all easy to use. Visit <http://www.dovepress.com/testimonials.php> to read real quotes from published authors.

Submit your manuscript here: <https://www.dovepress.com/international-journal-of-nanomedicine-journal>